Cell Reports
Physical Science

Article

An integrated, wearable paper microfluidic array device for multicomponent electrochemical sweat sensing

Graphical abstract

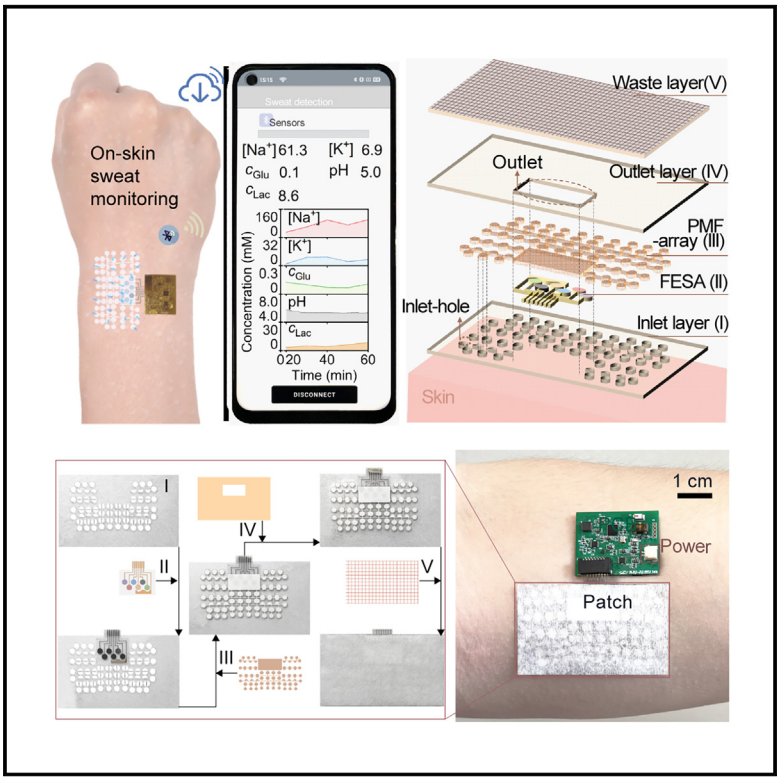

Highlights

- A PMF array adopting 96 inlets for efficient on-skin sweat sampling
- *In vitro* model of skin to test filling and refilling capability of sweat on PMF-array
- Real-time sweat sensing with sensor array fabricated by one-step drop coating
- Skin-mounted, wearable device for continuous dynamic analysis of 5 components in sweat

Authors

Qian Yu, Jie Wu, Wencheng Xiao, ..., Jun Zhou, Lin Ding, Huangxian Ju

Correspondence

hxju@nju.edu.cn

In brief

Yu et al. design a mass-producible paper microfluidic array with 96 inlets for efficient on-skin sweat sampling. This microfluidic array can be integrated with a flexible electrochemical sensing array, a printed circuit board, and an app to form a wearable device for continuous sweat collection and real-time multicomponent sensing.

Yu et al., 2025, Cell Reports Physical Science 6, 102389
January 15, 2025
https://doi.org/10.1016/j.xcrp.2024.102389

CellPress

Cell Reports
Physical Science

CellPress
OPEN ACCESS

Article

An integrated, wearable paper microfluidic array device for multicomponent electrochemical sweat sensing

Qian Yu,[1,3] Jie Wu,[1,3] Wencheng Xiao,[1] Chao Zhao,[2] Weiqi Zhang,[1] Yunlong Chen,[1] Ying Liu,[1] Hong Liu,[2] Jun Zhou,[1] Lin Ding,[1] and Huangxian Ju[1,4,*]

[1]State Key Laboratory of Analytical Chemistry for Life Science, School of Chemistry and Chemical Engineering, Nanjing University, Nanjing 210023, China

[2]State Key Laboratory of Digital Medical Engineering, Southeast University, Nanjing 210023, China

[3]These authors contributed equally

[4]Lead contact

*Correspondence: hxju@nju.edu.cn

https://doi.org/10.1016/j.xcrp.2024.102389

SUMMARY

Wearable sweat-sensing devices hold great promise for personalized healthcare but are facing substantial challenges in industrialization due to the lack of simple and efficient on-skin sweat-sampling modules. Here, we design a mass-producible paper microfluidic array with 96 inlets for tandem sweat collection, effective sampling (12 μL min^{-1}), and quick refilling (2 min). This microfluidic array can be conveniently worn on different parts of the body and integrated with a flexible electrochemical sensor array, which has been demonstrated with the newly developed array of Na^+, K^+, H^+, glucose, and lactate sensors, and a printed circuit board for Bluetooth-controlled signal processing. Continuous analysis of sweat metabolites and electrolytes can be achieved to directly visualize the results on a custom-smartphone app. On-body tests demonstrate the feasibility of this skin-mounted, wearable device for continuous perspiration collection and multicomponent monitoring, demonstrating its practical application prospects.

INTRODUCTION

Personalized healthcare is highly anticipated, as it can effectively enhance therapeutic efficacy and reduce medical risks and resources. Its implementation requires long-term and frequent monitoring and assessment of physiological parameters related to human health. Blood analysis is not the best selection to achieve this objective because it is invasive and episodic and often requires labor-intensive sample processing and delicate instrumentation.[1,2] Sweat contains abundant physiological and metabolic biomolecules that can be accessed non-invasively, continuously, and long term; thus, is has been considered as another attractive biofluid for health monitoring[3] and clinical diagnosis of cystic fibrosis, sweat gland dysfunction, and electrolyte balance.[4–6] However, the current sweat detection systems commonly employ off-body laboratory analysis and therefore do not have the advantages of simplicity, real time information, and ease of implementation.

Wearable sensors are a recently developed technology for remote, wireless, and real-time monitoring of an individual's health state by integrating analytical tools into a body-worn platform.[7] It has been achieved for the measurement of vital signs such as heart rate,[8] blood pressure,[9] and pulse.[10] Compared to physical sensing, wearable chemical sensing is more attractive for providing health information about the wearer at the molecular level.[11] Some wearable electrochemical sensing devices have been proposed for the on-body detection of metabolites (such as glucose, lactate, uric acid, alcohol, and caffeine),[12–16] electrolytes (such as Na^+, K^+, H^+, and Cl^-),[17,18] hormones (such as cortisol),[19] nutrients (such as amino acids and vitamins),[20] and neuroimmune[21,22] and inflammatory biomarkers (such as cholesterol and C-reactive protein)[23] in sweat. However, wearable sweat sensors are facing substantial challenges regarding widespread implementation and industrialization due to the lack of simple and efficient on-skin sweat sampling modules, though these sensing devices possess the inherent advantages and ability to continuously, *in situ*, and non-invasively measure a series of physiological molecules over a long period.[24,25]

Continuous on-skin sweat extraction is usually performed with iontophoresis[26] or sophisticated microfluidic technology.[27] The paper-based microfluidic (PMF) array is the most promising candidate for the construction of wearable sweat sensors owing to the intrinsic hydrophilicity,[28] breathability, flexibility, foldability, diversity, operational simplicity, and biodegradability of the paper.[29] Some functionalization strategies have also been used to endow the paper channels with the capabilities of oil adsorption,[30] osmotic extraction,[31] flow guidance,[32] and integration testing.[33–36] However, the common single-inlet sampling design greatly limits the efficiency of skin sweat extraction and,

thus, the practical application of these developed wearable sensing devices.

Here, we rationally design a PMF array with 96 inlets distributed across 8 interconnected input channels around the collection zone for efficient on-skin sweat sampling. This PMF array can be conveniently worn on different parts of the body and integrated with a flexible electrochemical sensor array to form a wearable patch for comfortable skin-mounted sweat collection and on-line multicomponent detection. By integration with a newly developed flexible electrochemical sensing array (FESA) for Na^+, K^+, H^+, glucose, and lactate, the obtained PMF array-based wearable device has following features: (1) low-cost mass fabrication of both the PMF array and FESA as well as their integration adaptable to industrialization; (2) long-term wearing robustness and comfort due to the separation of channels, collection zone, and FESA from the skin; (3) effective sampling and quick refilling of sweat for continuous multicomponent monitoring; and (4) good reliability of the Bluetooth-controlled signal processing along with real-time pH correction for enhancing the accuracy of sweat analysis. Therefore, this work solves the bottleneck of wearable sweat-sensing devices and their application in personalized healthcare.

RESULTS

Overview of the wearable device

The fully integrated wearable device consisted of three parts: a disposable multisensing patch, a reusable printed circuit board (PCB), and a user-friendly app. The patch containing the PMF array and FESA was attached to the skin for autonomous sweat collection and continuous detection, the PCB was interfaced with the patch for *in situ* signal processing and wireless communication with user's mobile device through Bluetooth, and the app was used to display and store the test results (Figure 1A). The PMF array was produced by laser engraving of normal filter paper (Figure S1) and consisted of two functional zones; namely, the harvesting zone, containing 24 circular and 72 semicircular inlets to efficiently extract sweat from a large area of skin, and the rectangular collection zone as a reservoir for FESA detection. The two zones were connected by 8 input channels (Figure 1B). The FESA was fabricated on a flexible thin-film electrode array, which contained five gold working electrodes (WEs) for the preparation of glucose, lactate, H^+, Na^+ and K^+ sensors; a silver electrode for preparing the shared Ag/AgCl reference electrode (RE); and a wave-shaped Au counter electrode (CE) for amperometric detection of glucose and lactate (Figures 1C, S2, and S3). The preparation of five sensors was performed by drop-coating a dispersion of glucose oxidase (GOx), Prussian blue nanoparticles (PBNPs), and multiwall carbon nanotubes (MCNTs) in 0.2% chitosan solution, a mixture of lactate dehydrogenase (LDH) and MCNTs in 0.15% chitosan, and selective membrane cocktails of H^+, Na^+, and K^+ on the WEs (Figure 1D). The patch was assembled by sequentially stacking the FESA (II), PMF array (III), outlet layer (IV), and waste layer (V) on the inlet layer (I) (Figures 1E and 1F). Here, both layers I and IV were double-sided medical adhesive tapes engraved with an array of inlet holes and a rectangular outlet, respectively. The FESA faced the collection zone of the PMF array, and all inlets of the PMF array were aligned one-to-one with the inlet holes of layer I.

After the patch was easily mounted on skin through adhesive layer I (Figure 1G), the inlets of the PMF array could directly contact the skin through the inlet holes of layer I for immediate extraction of sweat from the sweat glands. The PMF array showed a strong self-driving ability for extraction, transport, and collection of sweat due to the hygroscopicity and capillarity of the paper substrate (Figure 1H). The sweat in the collection zone could be discharged spontaneously in the presence of water-absorbent nonwoven cotton (waste layer), thus achieving continuous monitoring of sweat metabolites and electrolytes.

Design and optimization of the PMF array

The sweat extraction efficiency of the harvesting zone in the PMF array is a key factor to realize on-body analysis of sweat molecules. Sweat glands are spread throughout the body with varying densities of 90–550 glands cm^{-2}, and sweating occurs on all skin of the body, which leads to a large amount of whole-body perspiration (~1.6–100 mL min^{-1}) in spite of the relatively low sweat secretion rate (<20 nL $gland^{-1}$ min^{-1}).[37,38] Thus, this work designed a harvesting zone with multicircular and semicircular inlets for efficient tandem sweat collection from as many sweat glands as possible. The diameter of inlets, the number and length of input channels, the density of inlets, and the harvesting zone area were optimized for quick filling of the collection zone with sweat.

The diameter of inlets was optimized by probability analysis to match the skin sweat gland density and enable the highest sweat gland coverage efficiency (Figures 2A and S4A). At an average gland density of 150 gland cm^{-2} (forearm), the inlet area should be greater than 4 mm^2 (i.e., diameter > 2 mm) to ensure a 100% probability of covering one gland ($p \geq 1$) with random positioning. The probability of covering multiple sweat glands increases with increasing the inlet area. For example, an inlet area of 14 mm^2 (i.e., diameter = 4.2 mm) can maximize the probability of covering 10 sweat glands ($p \geq 10$) (Figure 2B). However, the threshold area of inlets for covering multiple sweat glands with 100% probability can be decreased by using the multi-inlet sampling model. For example, the threshold area of inlets for 100% $p \geq 10$ decreased to 7 mm^2 (i.e., diameter = 3 mm), when the inlet number is more than 8 (number of circular inlets [N_c] ≥ 8) (Figure 2C). Furthermore, the relativity of $p \geq 10$ to the inlet area in a series of multi-inlet sampling models (N_c from 1 to 116) at different gland densities indicates that an inlet area of 7 mm^2 (i.e., diameter = 3 mm) can guarantee 100% $p \geq 10$ under all gland densities for the sampling model of $N_c = 60$ (Figures 2D and S4B–S4D). Thus, an inlet diameter of 3 mm was selected for the PMF array.

Numerical simulation was used to optimize the number of input channels around the collection zone of 18 × 9 mm^2. The corners of the rectangular collection zone may form dead areas at too few entrances, leading to uneven dispersion and untimely refilling of sweat in the collection zone. With increasing entrance numbers, the dead area sharply decreases to a minimum value at more than 6 entrances (Figure 2E), which was demonstrated by filling green $CuCl_2$ solution in the collection zone (Figures S5 and S6). As expected, the filling time decreased significantly

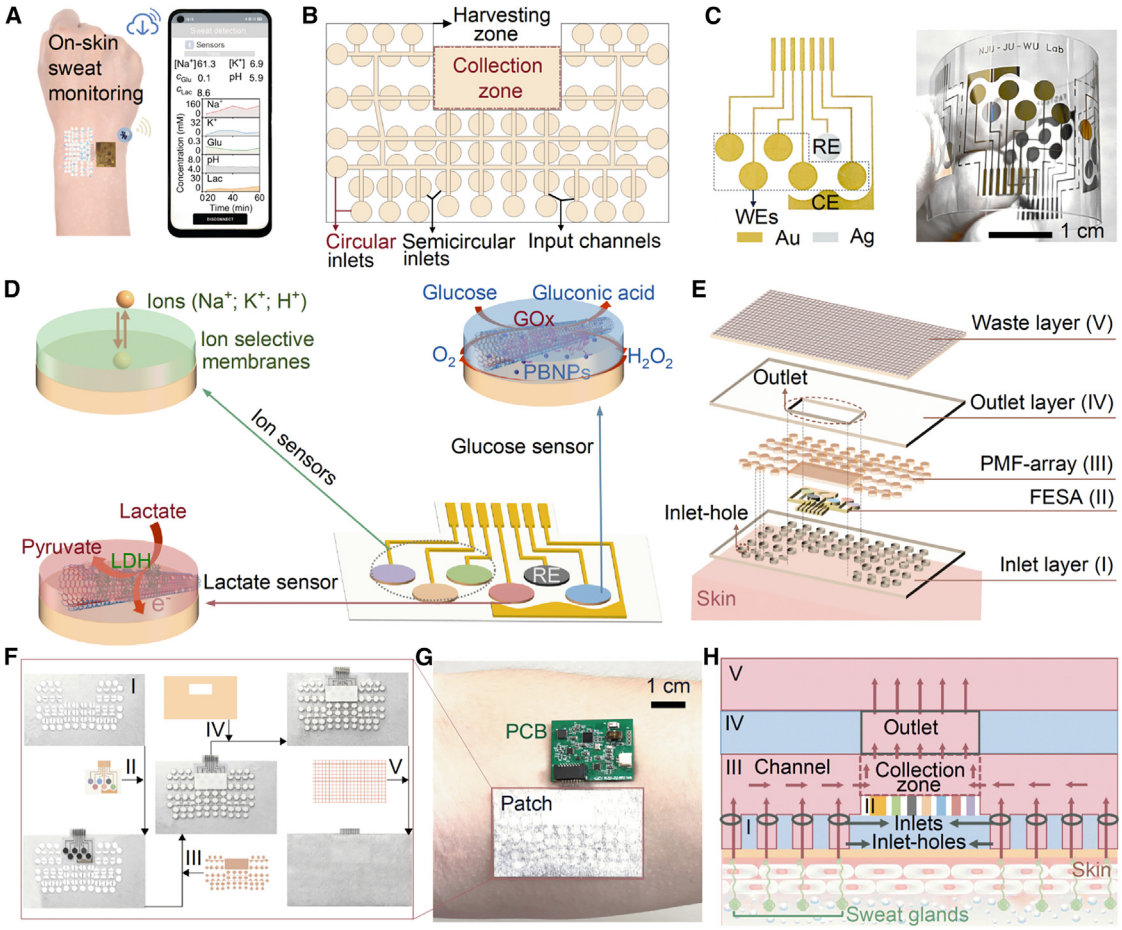

Figure 1. Schematics and images of the wearable device for sweat monitoring

(A) Schematic of the wearable device for on-skin sweat monitoring and mobile app for data display.

(B) Schematic of the PMF array.

(C) Schematic and image of a flexible thin-film electrode array. WE, working electrode; RE, reference electrode; CE, counter electrode. Scale bars, 1 cm.

(D) Schematic of an FESA containing glucose, lactate, Na^+, K^+, and H^+ sensors.

(E and F) Schematic (E) and images (F) of assembled layers in the wearable patch, which provides sealing conditions for sweat sampling and analysis without evaporation and contamination.

(G) Image of the wearable patch interfaced with a PCB mounted on the skin. Scale bars, 1 cm.

(H) Schematic of skin sweat sampling through the patch in cross-sectional view.

by increasing the number of input channels due to the increase of inlets (Figure 2F). Considering the spatial layout around the collection zone, 8 input channels were selected for the PMF array.

The effect of channel length on filling time indicated an optimal channel length of 12 mm and filling time of 10 min, and a longer channel led to a quick increase in filling time (Figures 2G and S7). The layout density of inlets around the collection zone was optimized at 8 input channels with 4-mm length and a harvesting area of ~4 cm^2. The filling time decreased sharply with the increasing inlet number (i.e., the density of inlets) and reached a minimum time of ~1 min at the saturated density of 4.4 N_c cm^{-2} (Figures 2H and S8). In order to achieve the highest sweat collection efficiency, the effect of harvesting area on filling time was examined. At the harvesting zone area of 11 cm^2 (i.e., 48 × 27 mm^2), where the inlet number was 60 (Figure S9), the filling time reached the minimum value of 25 s (Figure 2I). A larger harvesting area and number of inlets were insufficient to compensate for the time consumption due to the longer channels (Figure 2G). In addition, the channel width of 0.6 mm showed a shorter filling time than that of 1.0 mm (Figure 2J). At the optimal parameters, the PMF array structure with 0.6-mm channel width (Figure 2K) produced a sweat sampling rate of 12 μL min^{-1}, comparable to that of iontophoresis,[26] along with the uniform filling of sweat in the collection zone (Figures 2L and S10), indicating high sweat sampling efficiency.

The optimized PMF array exhibited good temporal resolution during filling or refilling of the collection zone, and the time-lapse images matched well with the simulation results (Figures 2M–2P; Table S1). The filling time of 25 s taken to reach 95% of the collection zone (Figures 2M and 2N; Video S1) was a significant improvement compared to the reported wearable sampling

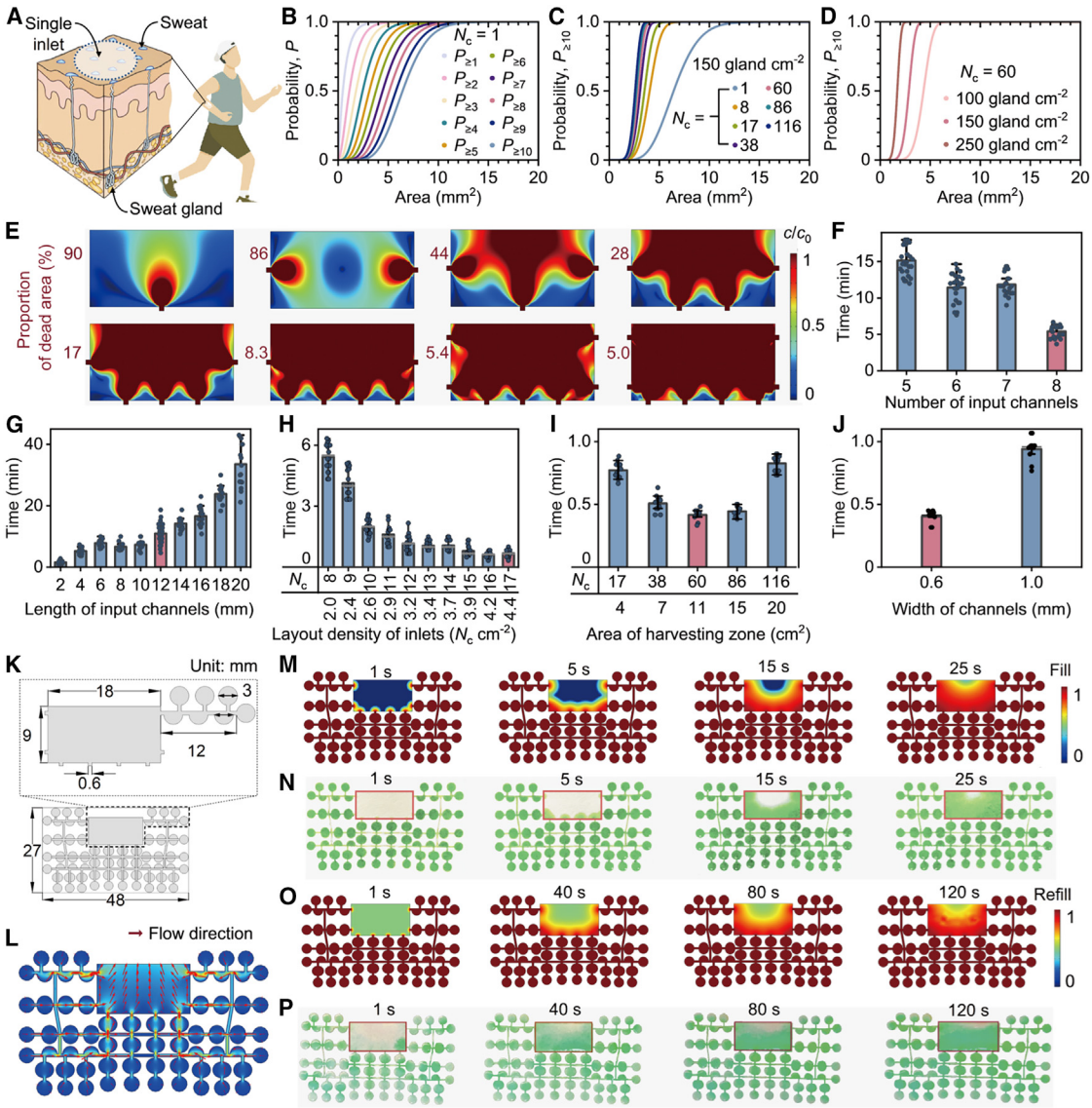

Figure 2. Characterization of the PMF array

(A) Schematic of the coverage of sweat glands in a single inlet.

(B) Probability of covering the number of sweat glands by an inlet as the function of inlet area in single-inlet sampling model (N_c = 1) at 150 gland cm^{-2}. $p \geq 1$ to $p \geq 10$ represent the probability of covering at least 1–10 sweat glands. N_c represents the number of circular inlets.

(C) Probability of covering at least 10 sweat glands by an inlet in the multi-inlets sampling model at 150 glands cm^{-2}.

(D) Effect of sweat gland density on the probability of covering at least 10 sweat glands at an N_c of 60.

(E) Numerically simulated proportion of the dead area at different numbers of entrances.

(F–J) Times requested to fill the collection zone with different numbers (F) and lengths (G) of input channels and different inlet densities (H), harvesting zone areas (I), and channel widths (J). Data are represented as mean ± SD of the measured data.

(K) Vector structure diagram of the PMF array.

(L) Simulation of the flow direction on the PMF array.

(M–P) Simulation of filling (M) and refilling (O) of NaCl solution in the collection zone and time-lapse images of filling of $CuCl_2$ solution on a dry (N) and refilling of $CuCl_2$ solution on a water-wetted (P) PMF array.

modules.[18,39] After a filled PMF array was placed below the dry waste layer for 1 min, the resulting half-filled PMF array showed a refilling time of 120 s (Figures 2O and 2P; Video S2). In order to demonstrate the feasibility of the PMF array for continuous monitoring, time-lapse analysis of the collection zone on a patch (Figure S11) under periodical fluid replacement sampling over a 1-h period was performed, which showed long-term usability and good stability of the PMF array (Figure S12). To simulate the real situation, an *in vitro* model of skin[40] was designed to test the filling time of the collection zone with low or medium sweat

rates and the capability of the periodic liquid replacement sampling of the PMF array (Figures S13–S16). The filling times for the collection area at low and medium sweat rates were 2 min and 45 s, respectively (Figures S14 and S15). Meanwhile, the periodic liquid replacement sampling experiment ensured continuous refilling of the collection zone under a low sweat rate (Figure S16), confirming the results shown in Figure S11. The prompt response and periodic change of signal corresponding to the fluid replacement indicated that the collection zone in the PMF array could be refreshed quickly and continuously, indicating an efficient on-skin sweat sampling module.

Fabrication and performance of the FESA

To ensure good detection reliability of the proposed wearable device, the FESA was designed to contain 5 sensors for simultaneous detection of Na^+, K^+, H^+, glucose, and lactate in sweat. The open-circuit potentials of ion sensors were recorded for Na^+, K^+, and H^+ detection, respectively. They exhibited sensitive Nernstian responses with the sensitivity of 76.9 mV decade^{-1} in 10–160 mM, 65.0 mV decade^{-1} in 1–32 mM, and −50.8 mV pH^{-1} at pH 4–7.8, respectively (Figures 3A–3C). All of these ion sensors showed good selectivity without cross-interference, long-term storage stability (Figure S17), and reversible testing performance (Figure S18). Five Na^+, K^+, and H^+ sensors prepared in different batches showed sensitivity variations of 1.9%, 4.5%, and 3.8%, respectively, indicating excellent reproducibility. Compared to the Na^+ and K^+ sensors fabricated by electrodepositing or coating PEDOT:PSS (poly(3,4-ethylenedioxythiophene)-poly(styrenesulfonate)) on an Au WE and then coating the Na^+- or K^+- selective membrane,[12,15,18] the Na^+ and K^+ sensors fabricated with one drop-coating step did not show the potential drift and sensitivity decrease (Figures S19A–S19D) due to the presence of the Au nanofilm (Figure S19E). The electron transfer impedance of Na^+ sensors fabricated with three procedures is shown in Figure S19F.

The glucose sensor prepared with a 3.4-μm film of 4-nm PBNP-adsorbed MCNTs (Figures 3D, 3E, and S20–S22) showed a linear response to glucose concentration ranging from 50 to 300 μM and a sensitivity of 1.3 nA μM^{-1} at 0 V (Figures 3F and S21), which was much better than those of the control sensors (Figure S23). For the preparation of the glucose sensor, the PBNPs were stabilized with PDDA (poly(diallyldimethylammonium chloride)) and CS (chitosan) (Figure S22) and then dispersed in 0.3 wt % chitosan for obtaining PBNP-adsorbed MCNTs. With the optimal composition (Figure S24), the glucose sensor could retain over 86% of its initial signal after 30-week storage and showed intra- and inter-batch sensitivity variations of 0.4% and 3.4%, respectively (Figure S25), indicating better stability than those in published works[12,41,42] and fabrication reproducibility.

The lactate sensor prepared with a 3.1-μm film of MCNTs/LDH showed a well-defined linear response over the tested concentration range of 0–30 mM with a sensitivity of 1.6 nA mM^{-1} (Figures 3G, 3H, and S26) and could be stored over 10 weeks without obvious signal loss, much longer than those fabricated with lactate oxidase.[12,31] The sensitivity variation of four lactate sensors demonstrated good fabrication reproducibility (Figure S27). Both the glucose and lactate sensors exhibited good selectivity, as no apparent signal was observed for non-target sweat metabolites at physiological levels (Figures 3F and 3H).

To verify the wearable detection performance of the FESA for sweat, artificial sweat samples with varying concentrations of each analyte were prepared (Table S2). All of these 5 sensors in the artificial sweat-filled collection zone showed detection sensitivities close to those obtained in buffer solution, with relative sensitivity errors less than 8% (Figures S28, 3A–3C, 3F, and 3H). As control, the FESA was examined under a sample-soaked paper and in flow injection sampling mode; it exhibited similar detection sensitivities to corresponding analytes over the same concentration ranges (Figure S29), indicating that the sampling mode did not obviously affect the performance of the FESA. In addition, K^+, Na^+, glucose, and lactate sensors on the FESA maintained negligible cross-interference for sweat analysis (Figures 3I, S30, and S31). The patch assembled with the FESA and PMF array could be stably stored for 1 month (Figure S32). Therefore, the FESA could be used for continuous monitoring of Na^+, K^+, H^+, glucose, and lactate during sweat collection and refilling.

pH correction of the FESA

The pH of human sweat varies from 4.5 to 7.5 among individuals and on different parts of the body. Therefore, both the stability of each sensor on the FESA at different pH levels and pH correction are important for ensuring the detection accuracy of the wearable sweat device. K^+, Na^+, and glucose sensors showed relatively steady responses to corresponding analytes upon varying pH (Figure 3J), indicating that they were pH insensitive, and it was unnecessary to correct the results. Contrarily, the lactate sensor showed significant differences in the current responses and the slopes of calibration curves at different pH levels (Figures 3J and S33), which was attributed to the production of H^+ during the lactate oxidation by LDH.[43] Integration of H^+ and lactate sensors on the FESA could conveniently achieve real-time correction of the lactate sensor (Figure 3K). For example, accurate and consistent lactate concentrations at different pH levels could be displayed after correcting the significantly overestimated readouts based on the calibration curve obtained at pH 7.0 (Figure 3L). The influence of temperature on the performance of ion sensors was minimal, but the enzyme sensors showed significant influence (Figure S34). Considering the relatively stable temperature of human skin around 37°C, the concentration readouts of glucose and lactate sensors for on-body experiments were performed, with the calibration curves obtained at 37°C.

On-body validation of the wearable device

The on-body sweat sensing performance of the fully integrated wearable device was evaluated by continuous detection of sweat Na^+, K^+, H^+, glucose, and lactate in human subjects during the constant-load cycling and running exercise. This patch-based wearable device could be comfortably worn on different parts of the body, such as the forearm, neck, back, and forehead, for sweat detection (Figure 4A), and the data could be transmitted to a mobile set via Bluetooth using an app. Figure 4B shows regional studies of sweat Na^+, K^+, H^+, glucose, and lactate on a female subject during a 1-h cycling exercise. The

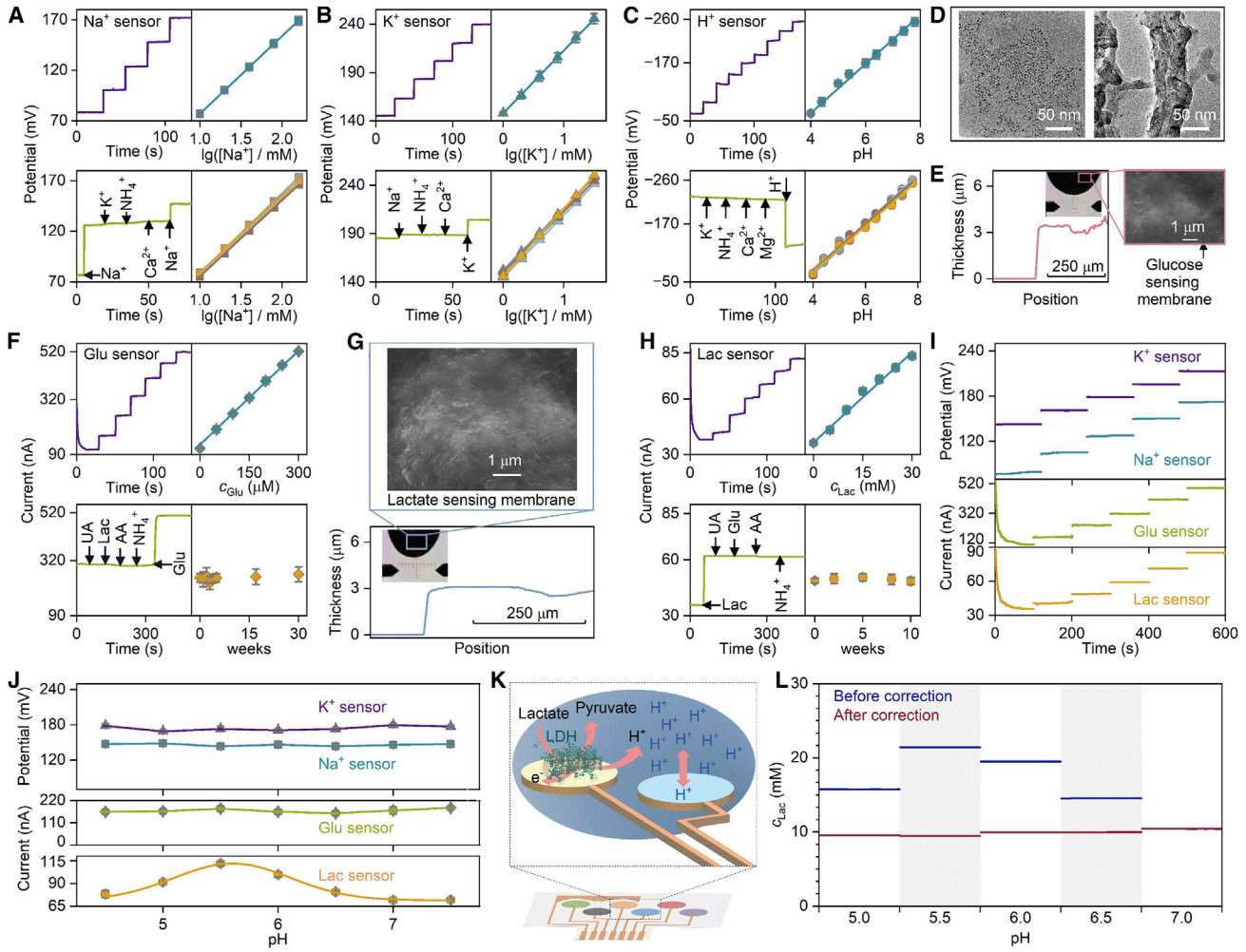

Figure 3. Characterization of the sensors on the FESA

(A–C) Open-circuit potentials, calibration curve, selectivity, and reproducibility of Na^+ (A), K^+ (B), and H^+ (C) sensors. Non-target interference concentration: 10 mM K^+, 50 mM Na^+, 5 mM NH_4^+, 0.5 mM Ca^{2+}, 0.5 mM Mg^{2+}. Data are represented as mean ± SD of the measured data.

(D) Scanning electron microscopy (SEM) images of PBNPs and PBNPs/MCNTs.

(E and G) SEM image and step profile of the glucose (E) and lactate (G) sensor and the sensing membrane on the Au electrode.

(F and H) Amperometric responses, calibration curve, selectivity, and stability of glucose (F) and lactate (H) sensors. Non-target interference concentration: 50 μM UA (uric acid), 50 μM AA (ascorbic acid), 5 mM lactate, 150 μM glucose. Data are represented as mean ± SD of the measured data.

(I) Simultaneous responses of K^+, Na^+, glucose, and lactate sensors on the FESA upon varying analyte concentrations.

(J) Influence of pH on the responses of corresponding sensors at 4 mM K^+, 80 mM Na^+, 30 μM glucose, and 20 mM lactate. Data are represented as mean ± SD of the measured data.

(K) Illustration of lactate oxidation catalyzed by the immobilized LDH and integration of lactate and H^+ sensors for pH correction.

(L) Concentration readout of 10 mM lactate based on the calibration curve obtained at pH 7.0 before and after pH correction.

levels as well as dynamic trends of all 5 sweat analytes in four regions exhibited good consistency, just with a slight advance or lag of the changes across different regions,[2] indicating that the regional differences in sweat detection could be ignored. Sweat glucose decreased for the forehead but decreased and then increased for other places. This was probably due to individual differences.

The accuracy of the wearable devices for analyzing real sweat samples was verified by recovery tests (Figures 4C–4F). The orthogonal regression analyses showed that all Na^+, K^+, glucose, and lactate sensors exhibited both good correlation coefficients (>0.99) and slopes close to 1, indicating good accuracy and reliability of patch-based sweat detection.

The wearable devices were further tested on 17 healthy subjects by wearing on the forearm during a running exercise (Figure 5A). The monitoring was triggered after 20 min of exercise and performed every 10 min to ensure sufficient sweat sampling for stable and reliable detection (Figure 5B). In order to reliably reveal the dynamic changes of Na^+, K^+, glucose, and lactate in sweat, their concentrations in the blood and the heart rate of the subjects were detected synchronously during the exercise. Meanwhile, group analysis of the 12 male and 5 female

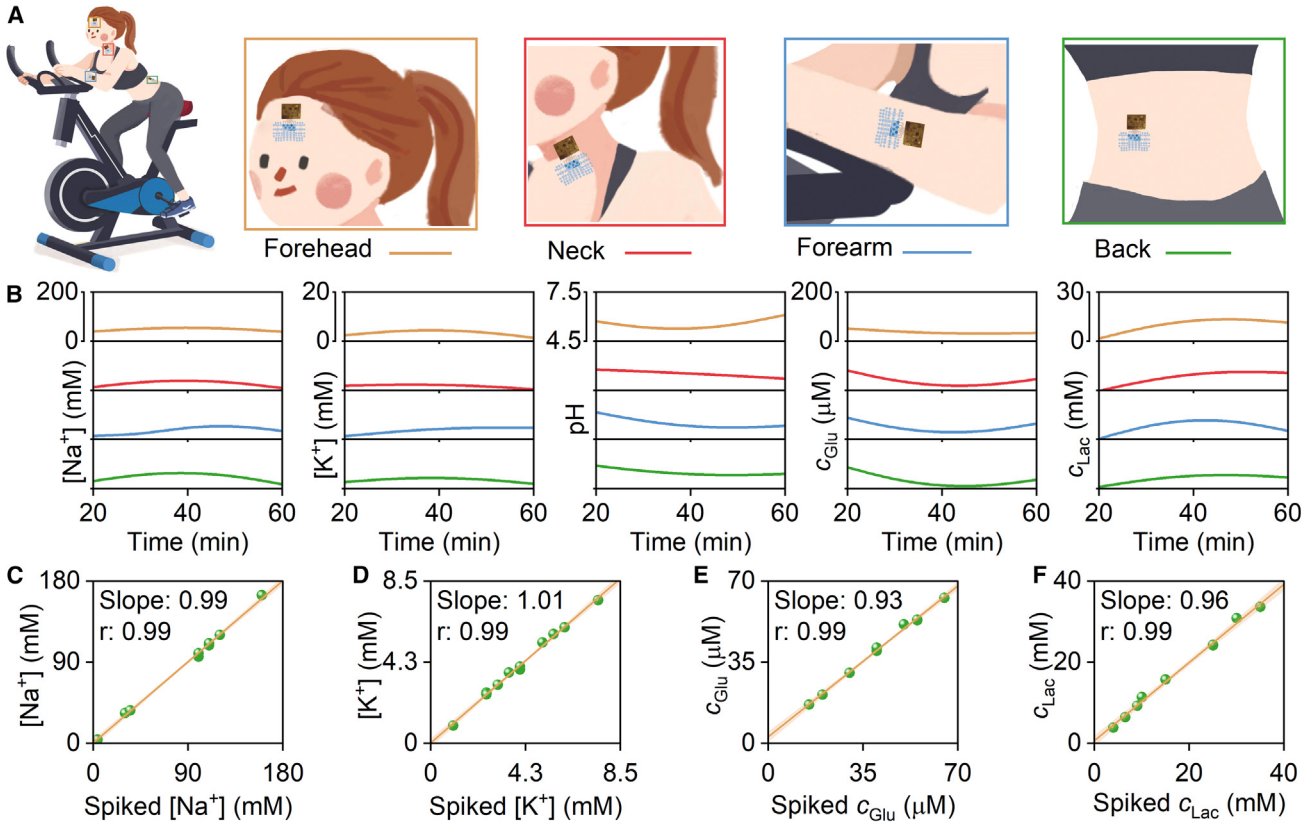

Figure 4. Validation of the wearable device

(A) Schematic of wearable devices worn on different parts of the body for sweat monitoring.

(B) Regional monitoring of Na^+, K^+, H^+, glucose, and lactate in sweat during a 1-h cycling exercise.

(C–F) Recovery tests of Na^+ (C), K^+ (D), glucose (E), and lactate (F) sensors by detecting Na^+, K^+, glucose, and lactate spiked in sweat samples.

participants was conducted to evaluate the effect of gender on dynamic changes of these sweat analytes (Figure 5C). The results indicated that the sweat pH of these 17 subjects fluctuated between 5.0 and 7.0. The dynamic changes of sweat Na^+ were heterogeneous in each individual, while an overall trend of first increasing and then slowly decreasing was observed for both males and females, and the fluctuation for females was earlier and more obvious than that for males. Compared to the sweat Na^+, blood Na^+ remained at a constant value at a high level throughout the entire exercise. Sweat K^+ showed a similar trend of first increasing and then decreasing as sweat Na^+, but male subjects exhibited a more pronounced fluctuation than females. Blood K^+ was also stable during exercise. Sweat glucose displayed an overall trend of first decreasing and then stabilizing on all subjects, but female subjects exhibited a greater decrease of sweat glucose than males during the entire exercise, which might be due to the higher density of sweat glands in females than in males.[44] Unlike the obvious fluctuations in sweat glucose, blood glucose remained stable during exercise. Sweat lactate gradually increased in the early stage of exercise and then returned to the initial state as the exercise progressed, while blood lactate did not show any significant change at the beginning of exercise but increased slowly and finally remained constant during exercise, regardless of gender.

The overall sweat-to-blood correlations of Na^+, K^+, glucose, and lactate across all subjects are illustrated in Figures 5D–5G. The sweat Na^+ was 2–7 times lower than blood Na^+, sweat K^+ was 1–2 times higher than blood K^+, sweat glucose was 30–100 times lower than blood glucose, and sweat lactate was 1–3 times higher than blood lactate. The poor Pearson correlation coefficients of 0.4, −0.2, 0.2, and 0.2 indicated that the sweat-to-blood correlations of Na^+, K^+, glucose, and lactate were mild.

DISCUSSION

To meet the demand of simple and efficient on-skin sweat sampling for wearable sweat sensing, this work designs a mass-producible paper microfluidic array. This PMF array is optimized to contain 24 circular and 72 semicircular inlets with a diameter of 3 mm, which are distributed across 8 interconnected input channels with 12-mm length and 0.6-mm width around a rectangular collection zone of 18 × 9 mm^2 and can be conveniently and comfortably worn on different parts of the body with a skin area of 424 mm^2. Different from previously reported sweat sampling structures, which usually included a single (or a few) mini-inlet(s) and could only collect limited sweat from very small skin areas,[39] the PMF array adopts 96

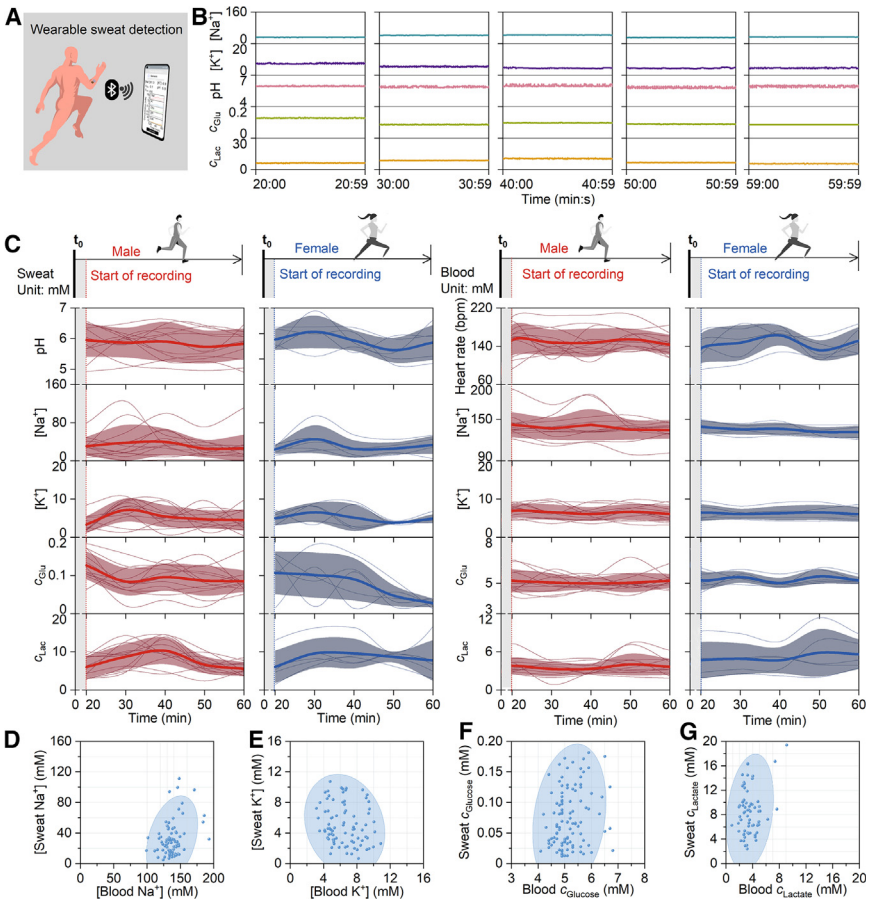

Figure 5. On-body sweat monitoring during continuous exercise for validation of the wearable device

(A) Illustration of sweat monitoring during the running exercise with the wearable device worn on the forearm.

(B) Simultaneous detection results of pH, Na^+, K^+, glucose, and lactate (mM) at different times.

(C) Simultaneous monitoring of Na^+, K^+, glucose, and lactate in sweat (and pH) and blood (and heat rate) during the 1-h running exercise with 12 male and 5 female participants. Thick solid lines and shaded bands indicate the mean ± SD of the 12 male and 5 female participants' measured data (red for male concentration values [and pH, heart rate], blue for female concentration values [and pH, heat rate]).

(D–G) Sweat-to-blood correlations of Na^+ (D), K^+ (E), glucose (F), and lactate (G) across all subjects.

inlets for achieving highly efficient on-skin sweat sampling (12 μL min^{-1}) and refilling (2 min), taking into account the gland density of 150 gland cm^{-2} and the sweat secretion rate of 20 nL $gland^{-1}$ min^{-1}.[37,38] The time-lapse analysis of the collection zone on a patch has demonstrated its long-term usability and good stability for continuous quick filling and refilling of sweat (Figures 2M–2P and S12–S15; Videos S1 and S2).

The designed on-skin sweat sampling module can be seamlessly installed with a FESA in the collection zone to form a wearable patch. After integrating the patch with a PCB and an app, a wearable device can be obtained for remote and wireless detection of sweat metabolites (glucose and lactate) and electrolytes (Na^+, K^+, and H^+) continuously. Compared to previous multistep technologies or the time-consuming electrodeposition method[12,26] for the preparation of a sensing array, the proposed one-step drop-coating method has demonstrated excellent reproducibility and mass production capacity of the sensing array. Moreover, LDH has been used for the preparation of the lactate sensor, which decreases the fabrication cost and leads to better stability over 2.5 months. The ion sensors on the FESA exhibit a stable Nernstian response without potential drift. All of the ion and amperometric sensors possess good selectivity without cross-interference.

The excellent performance of the FESA has been verified with the artificial sweat samples, which shows detection sensitivities similar to those observed for individual sensors in buffer solutions. Furthermore, the sampling mode does not obviously affect the performance, ensuring practical application of the FESA for continuous monitoring of these analytes during sweat collection and refilling. More importantly, K^+, Na^+, and glucose sensors are pH insensitive, and the combination of a lactate sensor with H^+ sensors on the FESA can be used for real-time pH correction of lactate detection (Figures 3K and 3L).

On-body and recovery tests have also demonstrated the feasibility and reliability of the proposed wearable device for continuous sweat sampling and dynamic Na^+, K^+, glucose, and lactate analysis during exercise. Interestingly, the continuous sweat detection on different parts of the body, such as the forearm, neck, back, and forehead, show good consistency of the 5 analyte levels as well as their dynamic trends. The levels of sweat Na^+, K^+, glucose, and lactate at the same part of the body show heterogeneous changes during the running exercise, which are different from those in the blood and depend on the gender, the individual, and exercise progress. Unfortunately, only mild sweat-to-blood correlations were observed due to a small number of human subjects. Therefore, a larger amount of human sweat data are still required to obtain clinical reference indicators for achieving application of sweat detection in personalized health assessment.

METHODS

Study design

The objective of this study was to develop a low-cost and scale-production paper microfluidic array for efficient on-skin sweat sampling and a wearable patch along with a flexible electrochemical sensor array for online multicomponent monitoring. The designed microfluidic array can be seamlessly integrated

with the newly developed FESA, a PCB, and an app to form a wearable device for wireless detection of sweat metabolites (glucose and lactate) and electrolytes (Na^+, K^+, and H^+). The healthy volunteers were recruited from the campus of Nanjing University through advertisement of on-body testing. On-body and recovery tests were performed to demonstrated the feasibility and reliability of the proposed wearable device for continuous, dynamic Na^+, K^+, H^+, glucose, and lactate analysis during exercise. Regional sweat studies on four parts of the body during a 1-h cycling exercise and group analysis of the 12 male and 5 female participants at the same part of the body during the 1-h running exercise were performed to verify the feasibility of using the on-skin biosensor in a clinical environment.

Preparation of the FESA

The sensing array was constructed on a flexible electrode array containing 5 Au WEs, an Ag electrode, and an Au CE (Figure 1C) and was fabricated on 100 μm PET (polyethylene terephthalate) by electronic beam evaporation (Ninghaijieyi Biotech, Ningbo, China).

Preparation of the glucose sensor: First, PBNPs were synthesized by dropwise addition of 4 mL of 0.025 M $K_3[Fe(CN)_6]$ to 16 mL of a mixture containing 6.25 mM $FeCl_2 \cdot 4H_2O$, 0.4 wt % PDDA, and 0.15 wt % chitosan under stirring for 1 h[45] and dispersion in 1 mL 0.3 wt % chitosan after centrifugation washing with 1% acetic acid. 250 μL of the dispersion was then mixed with 1.75 mL of 2 mg mL^{-1} MCNTs in 0.3 wt % chitosan and stirred overnight to obtain PBNP-adsorbed MCNTs (PBNP/MCNT), which were mixed thoroughly with 10 mg mL^{-1} GOx at a volume ratio of 2:1 to prepare the PBNP/MCNT/GOx dispersion. The glucose sensor was finally fabricated by coating 5 μL of PBNP/MCNT/GOx on the Au WE and drying at room temperature.

Preparation of the lactate sensor: After 3 mg mL^{-1} MCNTs (in 0.3 wt % chitosan) was mixed thoroughly with 10 mg mL^{-1} LDH at equal volume to obtain an MCNT/LDH dispersion, 5 μL of the dispersion was coated on the Au WE to prepare the lactate sensor.

Preparation of the H^+, Na^+, and K^+ sensors: Cyclohexanone was used as solvent to dissolve various components in an H^+-, Na^+-, and K^+-selective membrane cocktail. The H^+-selective membrane cocktail was prepared by dissolving 1 mg tridodecylamine, 0.55 mg Na-TFPB (sodium tetrakis[3,5-bis (trifluoromethyl)phenyl] borate), 33 mg PVC (high-molecular-weight polyvinyl chloride), and 65.45 mg DOS in 660 μL cyclohexanone.[46] The Na^+-selective membrane cocktail contained 1 mg Na ionophore X, 0.55 mg Na-TFPB, 33 mg PVC, and 65.45 mg DOS (bis(2-ethylhexyl) sebacate) in 660 μL of cyclohexanone,[47] while the K^+-selective membrane cocktail was prepared by dissolving 2 mg valinomycin, 0.5 mg NaTPB (sodium tetraphenylborate), 32.7 mg PVC, and 64.7 mg DOS in 350 μL cyclohexanone.[12] The ion sensors were then fabricated by casting 4 μL of the cocktails on the Au WEs.

Preparation of RE: Firstly, Ag/AgCl electrode was prepared by immersing the Ag electrode in 0.1 M $FeCl_3$ solution for 40 s. After rinsing with water and drying by N_2, the Ag/AgCl electrode was coated with 4 μL of methanol solution containing 0.315 mg PVB, 8.0 μg F127, 0.8 μg MCNTs and 0.20 mg NaCl to obtain RE.

Electrochemical measurements of the sensing array

The glucose and lactate sensors were used for amperometric (i-t) detection at 0 V, and the H^+, Na^+, and K^+ sensors were detected via open circuit potential measurement on a CHI 1040C electrochemical workstation (CH Instruments, USA).

Under wet paper: A rectangular filter paper (18 × 9 mm) was put on the surface of a sensing array. The electrochemical measurements were performed after dropping 20 μL of testing solution on the filter paper and waiting for 60 s (Figure S29A).

In a flow system: The PDMS flow device consisted of a 162-μL rectangular reservoir (18 × 9 × 1 mm^3) with an inlet and an outlet at the opposite ends. The reservoir was fully enclosed upon the active sensing area. The testing solutions contained different concentrations of glucose, lactate, Na^+, and K^+ in McIlvaine's buffer (pH 4.0–8.0) and were sequentially injected from a 750-μL sample loop into the flow device at a rate of 150 μL min^{-1} (Figure S29G).

Fabrication of the paper microfluidic array

The PMF array was fabricated by laser engraving (Optima-5070, Nanjing Chaohan Digital Machinery, China) on a filter paper. Its pattern was made using Laser Work v.6 software to form a rectangular collection zone (18 × 9 mm), 24 circular and 72 semicircular inlets (3 mm in diameter), and multiple capillary channels (0.6 mm in width) (Figures 1B and S1).

Assembly of the patch

Layers I and IV were made of commercial double-sided medical adhesive tape (<50 μm thickness). Layer I was an inlet layer engraved with an array of inlet holes corresponding to the inlet pattern of the harvesting network. Layer IV was an outlet layer engraved with a rectangular outlet corresponding to the collection pattern of the harvesting network. Layer V was a piece of water-absorbent nonwoven cotton. The inlet layer (I), FESA (II), PMF array (III), outlet layer (IV), and waste layer (V) were assembled in order (Figures 1E and 1F).

Fabrication of the PCB

The PCB module was designed using Altium Designer (Altium). It contained a miniaturized potentiostat using a digital-to-analog converter (AD5667, Analog Devices) and operational amplifiers (TLV9064, Texas Instruments) for amperometric and potential measurements, a microcontroller (nRF52840, Nordic Semiconductor) with an integrated Bluetooth module for data processing and wireless connection to a smartphone, and a lithium battery (3.7 V, 1,000 mAh, 12 h) for power supply.

Human subject recruitment

The on-body sweat testing on human subjects was carried out in compliance with the relevant laws and ethics regulations under a protocol that was approved by the Medical Ethics Subcommittee of Science and Technology Ethics Committee of Nanjing University (OAP20230821001). 17 healthy individuals (12 males and 5 females, age range 18–30) were recruited from the campus of Nanjing University through advertisement. All subjects gave written informed consent before participation in the study.

On-body testing of wearable device

For on-body sweat analysis, the subjects wearing the wearable device were asked to perform a 60-min stationary cycling or running exercise at 22°C in a ventilated setting. The wearable device was used to simultaneously detect glucose, lactate, Na^+, K^+, and H^+ after 20 min of exercise. The measurement was repeated every 10 min until the subject stopped the exercise. During the on-body trial, the data were recorded by PCB and sent wirelessly to a mobile phone via Bluetooth. The concentrations of glucose, lactate, Na^+, K^+, and H^+ obtained with the calibration curves were shown directly on a custom smartphone app. Meanwhile, sweat samples were collected periodically from the forearm of subjects using centrifuge tubes for further validation of the detection accuracy by recovery tests (Figures 4C–4F).

Synchronous blood analysis

For the human trials, blood glucose, lactate, Na^+, and K^+ were tested before exercise and then tested periodically every 10 min. The blood samples were obtained through a finger-prick approach after cleaning the fingertip with an alcohol wipe and allowing it to air dry. Blood glucose levels were recorded immediately with a commercial glucometer (Bayer). Meanwhile, fresh capillary blood samples were collected from the fingertips into Li-EDTA and gel tubes after wiping off the first drop of blood with a cotton swab. After centrifuging blood samples for 10 min, plasma samples were obtained for further analysis of blood lactate with a lactic acid assay kit (Nanjing Jiancheng Bioengineering Institute, China) and blood Na^+ and K^+ levels with the FESA by standard addition method.

Statistical analysis

Data are presented with average values and SD unless noted otherwise in the figure legends. The highest sweat gland coverage efficiency was obtained using probability analysis. All statistical analyses and linear regression analysis were performed using Origin software.

RESOURCE AVAILABILITY

Lead contact

Requests for further information, resources, and materials will be fulfilled by the lead contact, Huangxian Ju (hxju@nju.edu.cn).

Materials availability

This study did not generate new materials.

Data and code availability

This paper analyzes existing, publicly available data, accessible at [DOI: 10.1016/j.xcrp.202X.XX.XX]. All data reported in this paper will be shared by the lead contact upon request. This paper does not report original code. Any additional information required to reanalyze the data reported in this paper is available from the lead contact upon request.

ACKNOWLEDGMENTS

We gratefully acknowledge the National Natural Science Foundation of China (21890741, 21827812, and 21635005).

AUTHOR CONTRIBUTIONS

Q.Y., J.W., and H.J. proposed the idea and designed the experiments. Q.Y., Y.C., Y.L., J.Z., L.D., J.W., and H.J. wrote the manuscript. Q.Y. carried out the synthesis and electrochemical experiments. C.Z. and H.L. fabricated the PCB and app. W.Z. helped with electrochemistry measurements. W.X. helped with theoretical simulation of sweat wicking. All authors discussed the results and commented on the manuscript.

DECLARATION OF INTERESTS

The authors declare no competing interests.

SUPPLEMENTAL INFORMATION

Supplemental information can be found online at https://doi.org/10.1016/j.xcrp.2024.102389.

Received: October 18, 2024
Revised: November 21, 2024
Accepted: December 16, 2024
Published: January 15, 2025

REFERENCES

1. Adeel, M., Cotur, Y., Naik, A., Gonzalez-Macia, L., and Güder, F. (2022). Face masks as a platform for wearable sensors. Nat. Electron. *5*, 719–720. https://doi.org/10.1038/s41928-022-00871-2.
2. Anastasova, S., Crewther, B., Bembnowicz, P., Curto, V., Ip, H.M., Rosa, B., and Yang, G.Z. (2017). A wearable multisensing patch for continuous sweat monitoring. Biosens. Bioelectron. *93*, 139–145. https://doi.org/10.1016/j.bios.2016.09.038.
3. Yang, D.S., Ghaffari, R., and Rogers, J.A. (2023). Sweat as a diagnostic biofluid. Science *379*, 760–761. https://doi.org/10.1126/science.abq5916.
4. Di Sant'Agnese, P.A., Darling, R.C., Perera, G.A., and Shea, E. (1953). Abnormal electrolyte composition of sweat in cystic fibrosis of the pancreas; clinical significance and relationship to the disease. Pediatrics *12*, 549–563. https://doi.org/10.1542/peds.12.5.549.
5. Illigens, B.M.W., and Gibbons, C.H. (2009). Sweat testing to evaluate autonomic function. Clin. Auton. Res. *19*, 79–87. https://doi.org/10.1007/s10286-008-0506-8.
6. Sontag, M.K. (2016). Sweat chloride: the critical biomarker for cystic fibrosis trials. Am. J. Resp. Crit. Care. *194*, 1311–1313. https://doi.org/10.1164/rccm.201606-1286ED.
7. Ates, H.C., Nguyen, P.Q., Gonzalez-Macia, L., Morales-Narváez, E., Güder, F., Collins, J.J., and Dincer, C. (2022). End-to-end design of wearable sensors. Nat. Rev. Mater. *7*, 887–907. https://doi.org/10.1038/s41578-022-00460-x.
8. Bent, B., Goldstein, B.A., Kibbe, W.A., and Dunn, J.P. (2020). Investigating sources of inaccuracy in wearable optical heart rate sensors. NPJ Digit. Med. *3*, 18. https://doi.org/10.1038/s41746-020-0226-6.
9. Yi, Z., Liu, Z., Li, W., Ruan, T., Chen, X., Liu, J., Yang, B., and Zhang, W. (2022). Piezoelectric dynamics of arterial pulse for wearable continuous blood pressure monitoring. Adv. Mater. *34*, 2110291. https://doi.org/10.1002/adma.202110291.
10. Meng, K., Xiao, X., Wei, W., Chen, G., Nashalian, A., Shen, S., Xiao, X., and Chen, J. (2022). Wearable pressure sensors for pulse wave monitoring. Adv. Mater. *34*, 2109357. https://doi.org/10.1002/adma.202109357.
11. Kim, J., Campbell, A.S., de Ávila, B.E.F., and Wang, J. (2019). Wearable biosensors for healthcare monitoring. Nat. Biotechnol. *37*, 389–406. https://doi.org/10.1038/s41587-019-0045-y.
12. Gao, W., Emaminejad, S., Nyein, H.Y.Y., Challa, S., Chen, K., Peck, A., Fahad, H.M., Ota, H., Shiraki, H., Kiriya, D., et al. (2016). Fully integrated

wearable sensor arrays for multiplexed in situ perspiration analysis. Nature *529*, 509–514. https://doi.org/10.1038/nature16521.

13. Xiao, J., Luo, Y., Su, L., Lu, J., Han, W., Xu, T., and Zhang, X. (2022). Hydrophilic metal-organic frameworks integrated uricase for wearable detection of sweat uric acid. Anal. Chim. Acta *1208*, 339843. https://doi.org/10.1016/j.aca.2022.339843.
14. Sun, M., Pei, X., Xin, T., Liu, J., Ma, C., Cao, M., and Zhou, M. (2022). A flexible microfluidic chip-based universal fully integrated nanoelectronic system with point-of-care raw sweat, tears, or saliva glucose monitoring for potential noninvasive glucose management. Anal. Chem. *94*, 1890–1900. https://doi.org/10.1021/acs.analchem.1c05174.
15. Wang, J., Wang, L., Li, G., Yan, D., Liu, C., Xu, T., and Zhang, X. (2022). Ultra-small wearable flexible biosensor for continuous sweat analysis. ACS Sens. *7*, 3102–3107. https://doi.org/10.1021/acssensors.2c01533.
16. Zhang, X., Tang, Y., Wu, H., Wang, Y., Niu, L., and Li, F. (2022). Integrated aptasensor array for sweat drug analysis. Anal. Chem. *94*, 7936–7943. https://doi.org/10.1021/acs.analchem.2c00736.
17. Chen, L., Chen, F., Liu, G., Lin, H., Bao, Y., Han, D., Wang, W., Ma, Y., Zhang, B., and Niu, L. (2022). Superhydrophobic functionalized $Ti_3C_2T_x$ MXene-based skin-attachable and wearable electrochemical pH sensor for real-time sweat detection. Anal. Chem. *94*, 7319–7328. https://doi.org/10.1021/acs.analchem.2c00684.
18. Pei, X., Sun, M., Wang, J., Bai, J., Bo, X., and Zhou, M. (2022). A bifunctional fully integrated wearable tracker for epidermal sweat and wound exudate multiple biomarkers monitoring. Small *18*, 2205061. https://doi.org/10.1002/smll.202205061.
19. Torrente-Rodríguez, R.M., Tu, J.B., Yang, Y.R., Min, J.H., Wang, M.Q., Song, Y., Yu, Y., Xu, C.H., Ye, C., IsHak, W.W., et al. (2020). Investigation of cortisol dynamics in human sweat using a graphene-based wireless mHealth system. Matter *2*, 1–17. https://doi.org/10.1016/j.matt.2020.01.021.
20. Wang, M., Yang, Y., Min, J., Song, Y., Tu, J., Mukasa, D., Ye, C., Xu, C., Heflin, N., McCune, J.S., et al. (2022). A wearable electrochemical biosensor for the monitoring of metabolites and nutrients. Nat. Biomed. Eng. *6*, 1225–1235. https://doi.org/10.1038/s41551-022-00916-z.
21. Li, J., Liu, Y., Yuan, L., Zhang, B., Bishop, E.S., Wang, K., Tang, J., Zheng, Y.Q., Xu, W., Niu, S., et al. (2022). A tissue-like neurotransmitter sensor for the brain and gut. Nature *606*, 94–101. https://doi.org/10.1038/s41586-022-04615-2.
22. Jiang, Y., Trotsyuk, A.A., Niu, S., Henn, D., Chen, K., Shih, C.-C., Larson, M.R., Mermin-Bunnell, A.M., Mittal, S., Lai, J.-C., et al. (2023). Wireless, closed-loop, smart bandage with integrated sensors and stimulators for advanced wound care and accelerated healing. Nat. Biotechnol. *41*, 652–662. https://doi.org/10.1038/s41587-022-01528-3.
23. Tu, J., Min, J., Song, Y., Xu, C., Li, J., Moore, J., Hanson, J., Hu, E., Parimon, T., Wang, T.-Y., et al. (2023). A wireless patch for the monitoring of C-reactive protein in sweat. Nat. Biomed. Eng. *7*, 1293–1306. https://doi.org/10.1038/s41551-023-01059-5.
24. Shen, H., Xue, L., Ma, Y., Huang, H., and Chen, L. (2023). Recent advances toward wearable sweat monitoring systems. Adv. Mater. Technol. *8*, 2200513. https://doi.org/10.1002/admt.202200513.
25. Wu, J., Liu, H., Chen, W., Ma, B., and Ju, H. (2023). Device integration of electrochemical biosensors. Nat. Rev. Bioeng. *1*, 346–360. https://doi.org/10.1038/s44222-023-00032-w.
26. Emaminejad, S., Gao, W., Wu, E., Davies, Z.A., Yin Yin Nyein, H., Challa, S., Ryan, S.P., Fahad, H.M., Chen, K., Shahpar, Z., et al. (2017). Autonomous sweat extraction and analysis applied to cystic fibrosis and glucose monitoring using a fully integrated wearable platform. Proc. Natl. Acad. Sci. USA *114*, 4625–4630. https://doi.org/10.1073/pnas.1701740114.
27. Bandodkar, A.J., Gutruf, P., Choi, J., Lee, K., Sekine, Y., Reeder, J.T., Jeang, W.J., Aranyosi, A.J., Lee, S.P., Model, J.B., et al. (2019). Battery-free, skin-interfaced microfluidic/electronic systems for simultaneous electrochemical, colorimetric, and volumetric analysis of sweat. Sci. Adv. *5*, eaav3294. https://doi.org/10.1126/sciadv.aav3294.
28. Deroco, P.B., Junior, D.W., and Kubota, L.T. (2023). Paper-based wearable electrochemical sensors: a new generation of analytical devices. Electroanalysis *35*, 2200177. https://doi.org/10.1002/elan.202200177.
29. Ye, Z., Yuan, Y., Zhan, S., Liu, W., Fang, L., and Li, T. (2023). Paper-based microfluidics in sweat detection: from design to application. Analyst *148*, 1175–1188. https://doi.org/10.1039/D2AN01818G.
30. Yang, M., Sun, N., Lai, X., Wu, J., Wu, L., Zhao, X., and Feng, L. (2023). Paper-based sandwich-structured wearable sensor with sebum filtering for continuous detection of sweat pH. ACS Sens. *8*, 176–186. https://doi.org/10.1021/acssensors.2c02016.
31. Saha, T., Songkakul, T., Knisely, C.T., Yokus, M.A., Daniele, M.A., Dickey, M.D., Bozkurt, A., and Velev, O.D. (2022). Wireless wearable electrochemical sensing platform with zero-power osmotic sweat extraction for continuous lactate monitoring. ACS Sens. *7*, 2037–2048. https://doi.org/10.1021/acssensors.2c00830.
32. Mogera, U., Guo, H., Namkoong, M., Rahman, M.S., Nguyen, T., and Tian, L. (2022). Wearable plasmonic paper-based microfluidics for continuous sweat analysis. Sci. Adv. *8*, eabn1736. https://doi.org/10.1126/sciadvabn1736.
33. Li, M., Wang, L., Liu, R., Li, J., Zhang, Q., Shi, G., Li, Y., Hou, C., and Wang, H. (2021). A highly integrated sensing paper for wearable electrochemical sweat analysis. Biosens. Bioelectron. *174*, 112828. https://doi.org/10.1016/j.bios.2020.112828.
34. Li, T., Liang, B., Ye, Z., Zhang, L., Xu, S., Tu, T., Zhang, Y., Cai, Y., Zhang, B., Fang, L., et al. (2022). An integrated and conductive hydrogel-paper patch for simultaneous sensing of Chemical–Electrophysiological signals. Biosens. Bioelectron. *198*, 113855. https://doi.org/10.1016/j.bios.2021.113855.
35. Liang, B., Cao, Q., Mao, X., Pan, W., Tu, T., Fang, L., and Ye, X. (2021). An integrated paper-based microfluidic device for real-time sweat potassium monitoring. IEEE Sens. J. *21*, 9642–9648. https://doi.org/10.1109/JSEN.2020.3009327.
36. Cao, Q., Liang, B., Tu, T., Wei, J., Fang, L., and Ye, X. (2019). Three-dimensional paper-based microfluidic electrochemical integrated devices (3D-PMED) for wearable electrochemical glucose detection. RSC Adv. *9*, 5674–5681. https://doi.org/10.1039/c8ra09157a.
37. Martín, A., Kim, J., Kurniawan, J.F., Sempionatto, J.R., Moreto, J.R., Tang, G., Campbell, A.S., Shin, A., Lee, M.Y., Liu, X., and Wang, J. (2017). Epidermal microfluidic electrochemical detection system: enhanced sweat sampling and metabolite detection. ACS Sens. *2*, 1860–1868. https://doi.org/10.1021/acssensors.7b00729.
38. Sonner, Z., Wilder, E., Heikenfeld, J., Kasting, G., Beyette, F., Swaile, D., Sherman, F., Joyce, J., Hagen, J., Kelley-Loughnane, N., and Naik, R. (2015). The microfluidics of the eccrine sweat gland, including biomarker partitioning, transport, and biosensing implications. Biomicrofluidics *9*, 031301. https://doi.org/10.1063/1.4921039.
39. Bariya, M., Nyein, H.Y.Y., and Javey, A. (2018). Wearable sweat sensors. Nat. Electron. *1*, 160–171. https://doi.org/10.1038/s41928-018-0043-y.
40. Hou, L., Hagen, J., Wang, X., Papautsky, I., Naik, R., Kelley-Loughnane, N., and Heikenfeld, J. (2013). Artificial microfluidic skin for in vitro perspiration simulation and testing. Lab Chip *13*, 1868–1875. https://doi.org/10.1039/C3LC41231H.
41. Bai, J., Liu, D., Tian, X., Wang, Y., Cui, B., Yang, Y., Dai, S., Lin, W., Zhu, J., Wang, J., et al. (2024). Coin-sized, fully integrated, and minimally invasive continuous glucose monitoring system based on organic electrochemical transistors. Sci. Adv. *10*, eadl1856. https://doi.org/10.1126/sciadv.adl1856.
42. Xu, C., Song, Y., Sempionatto, J.R., Solomon, S.A., Yu, Y., Nyein, H.Y.Y., Tay, R.Y., Li, J., Heng, W., Min, J., et al. (2024). A physicochemical-sensing electronic skin for stress response monitoring. Nat. Electron. *7*, 168–179. https://doi.org/10.1038/s41928-023-01116-6.

43. Narayanan, J.S., and Slaughter, G. (2020). Lactic acid biosensor based on lactate dehydrogenase immobilized on Au nanoparticle modified microwire electrode. IEEE Sens. J. *20*, 4034–4040. https://doi.org/10.1109/JSEN.2019.2963405.

44. Green, J.M., Bishop, P.A., Muir, I.H., and Lomax, R.G. (2000). Gender differences in sweat lactate. Eur. J. Appl. Physiol. *82*, 230–235. https://doi.org/10.1007/s004210050676.

45. Chen, S., Yuan, R., Chai, Y., Xu, Y., Min, L., and Li, N. (2008). A new antibody immobilization technique based on organic polymers protected Prussian blue nanoparticles and gold colloidal nanoparticles for amperometric immunosensors. Sens. Actuators, B *135*, 236–244. https://doi.org/10.1016/j.snb.2008.08.032.

46. Oesch, U., Brzózka, Z., Xu, A., Rusterholz, B., Suter, G., Pham, H.V., Welti, D., Ammann, D., Pretsch, E., and Simon, W. (1986). Design of neutral hydrogen ion carriers for solvent polymeric membrane electrodes of selected pH range. Anal. Chem. *58*, 2285–2289. https://doi.org/10.1021/ac00124a037.

47. Bandodkar, A.J., Molinnus, D., Mirza, O., Guinovart, T., Windmiller, J.R., Valdés-Ramírez, G., Andrade, F.J., Schöning, M.J., and Wang, J. (2014). Epidermal tattoo potentiometric sodium sensors with wireless signal transduction for continuous non-invasive sweat monitoring. Biosens. Bioelectron. *54*, 603–609. https://doi.org/10.1016/j.bios.2013.11.039.